SLAC-PUB-1585
May 1975
(T/E)

ANALYSIS OF PARTICLE PRODUCTION AT LARGE TRANSVERSE MOMENTUM*

R. Blankenbecler and S. J. Brodsky

Stanford Linear Accelerator Center
Stanford University, Stanford, California 94305

and

J. Gunion†

Department of Physics, University of Pittsburgh
Pittsburgh, Pennsylvania 15260

ABSTRACT

An analysis of large transverse momentum data is carried out using local exponents which characterize the dependence of the cross sections on p_T and ϵ = (missing mass)^2/s. The results of this effective-power analysis allow any model to be critically compared to the data in a simple but meaningful way. Selected models are examined. A survey of the features of the Constituent Interchange Model is given for inclusive scattering, and some special features for electromagnetic processes are discussed. The CIM can explain, in a simple way, not only the behavior of the local exponents but also their specific values for each particle type using the quark counting rules. Quasielastic peaks in the ϵ distribution are observed for the difference between particle and antiparticle production (p-$\bar{p}$, K^+-K^-) which are consistent with expectations. Further crucial tests of the CIM are discussed.

(Submitted to Phys. Rev.)

* Work supported by the U.S. Energy Research and Development Administration.
† Supported by the National Science Foundation.

I. INTRODUCTION

One of the most important questions in strong interaction physics is whether particle production at large transverse momentum directly reflects the interactions of hadronic constituents at short distances. In the case of deep inelastic lepton scattering, Bjorken scaling implies that a finite fraction of a nucleon's momentum is carried by pointlike constituents.[1] Accordingly, in the case of hadronic collisions, one expects that particles can be produced at large transverse momentum by a single, hard, large-angle scattering involving these constituents.[2] The application of the hard-scattering constituent models to both exclusive[3-6] and inclusive processes[2,7-10] at high transverse momentum has in fact proven very fruitful.[11] On the other hand, more conventional - strictly hadronic - descriptions have also been utilized, including the multiperipheral,[12] fireball,[13] hydrodynamic,[14] and eikonal[15] models. Each type of approach has had some success in describing some portion of the first available inclusive data; however, with the advent of detailed single particle inclusive data from the CERN-ISR[16,17] and FNAL[18] for a variety of particle types, more significant and stringent tests of the basic dynamical mechanisms and the internal consistency of any given model have become possible.

We have found that among the most sensitive experimental parameters and discriminants of various models are the effective powers N_{eff} and F_{eff} defined in Eq. (I.3). In the remainder of this section we discuss the motivation for these parameters, and outline the general features of the hard-scattering models. In Section II, the data are analyzed in such a way as to reveal the basic features and systematic trends. The results of the effective power analysis allow any model to be critically compared with the data in a simple but meaningful way. In Section II, selected models are examined in light of the above analysis. They

are found to either disagree with the data, or to be incompletely developed. Section IV will summarize the essential features of the constituent interchange model (CIM)[3-4,7-9] while in Section V the physical interpretation of certain features of the theory will be discussed in detail. Section VI is devoted to a comparison with the data. The CIM is found to reproduce most features of the data in a natural way, though in some reactions several alternative CIM mechanisms are equally viable. In Section VI, the type and quality of additional experiments needed to completely specify the appropriate mechanism and to definitively test the model are discussed. In particular, the importance of correlation and angular dependence measurements, and of data taken with a variety of incident beams, is stressed.

All of the parton and "hard-scattering" models which have been proposed to describe hadron processes ($A + B \rightarrow C + X$) at large transverse momentum have the common underlying structure illustrated in Fig. 1. In fact, many conventional models also display a similar structure. In the hard-scattering models, the large transverse momentum reaction is assumed to occur as a result of a single large angle scattering $a + b \rightarrow c + d$ of constituents a and b, followed in general by the decay or fragmentation of c into the observed particle C. Particular models differ mainly by the choice of the "active" particles of systems a, b, c and d. In the model of Refs. 2 and 19, the active particles are assumed to be quarks. In the constituent interchange model,[7-9] the underlying large angle reaction involves quark-hadron scattering. In the multiperipheral models of Refs. 12, the large angle process involves only hadrons. Conceivably all three types of reactions could be involved.[20] Alternatively, it could be that, when fully formulated, portions of the various descriptions will phenomenologically prove equivalent. Indeed to the extent that quarks do not appear in the

final state some description in terms of purely hadronic final states must be possible. Explicit models in which this calculational equivalence occurs are, however, still missing, although "bag" models would appear to have the necessary separation between short and long distance behaviors.

The calculation of the cross section corresponding to Fig. 1 takes a simple probabilistic form for large p_T^2:

$$E\frac{d\sigma}{d^3p}(A + B \to C + X) \cong \sum_{a,b,c} \int_0^1 dx_a \int_0^1 dx_b \int_0^1 \frac{dx_C}{x_C^2} G_{a/A}(x_a)\, G_{b/B}(x_b)\, \tilde{G}_{C/c}(x_C)\, \delta(s'+t'+u')\frac{s'}{\pi}\frac{d\sigma}{dt'}(a+b\to c+d^*)\Bigg|_{\substack{s'=x_a x_b s\\ t'=x_a t/x_C\\ u'=x_b u/x_C}} \tag{I. 1}$$

Here $G_{a/A}(x_a)$ is the probability for the constituent or fragment a to have fractional longitudinal momentum x_a in a frame where $|p_A| \to \infty$; for quarks the Bjorken scaling function is $\nu W_{2A}(x) = \sum_q e_q^2 x\, G_{q/A}(x)$, with $x = -q^2/2m\nu$. Eq. (I. 1) was derived for specific cases by Berman, Bjorken, and Kogut[2] and has been developed in various forms by various authors. It can be derived using infinite-momentum frame methods,[7] or directly from a covariant analysis using light-cone[9] or Sudakov variables,[8] or via generalizations of the multiperipheral model.[12] Note that in case where A, B, or C is an active particle, we can use $G_{A/A}(x) \propto \delta(1-x)$, etc. We ignore absorption which, if present, affects only the cross section normalization.

In order to describe the cross section following from the above form, it is necessary to introduce kinematic variables and for convenience we choose s, $x_1 = -u/s$, $x_2 = -t/s$, $\epsilon = M^2/s \cong 1 - x_1 - x_2$, and $p_T^2 = x_1 x_2 s$. At 90° in the center of mass, another useful variable is $x_T = 2\, p_T/s^{\frac{1}{2}} \simeq 2x_1 = 2x_2$, and

$\epsilon = 1 - x_T$. Though the most convenient parametrization of the predictions will depend on the particular forms employed for the G's and $d\sigma/dt$, we choose to be guided by models with power law behavior for both functions.[3-10] Since the dimensionless G's can be assumed to be scale independent, the p_T dependence is determined by the fixed angle scaling behavior of $d\sigma/dt$. Taking $d\sigma/dt \sim s^{-N} f(\theta_{c.m.})$, this yields cross sections of the asymptotic form

$$E \frac{d\sigma}{d^3p} \sim \sum_{abc} \epsilon^F (p_T^2 + m^2)^{-N} I(x_1, x_2) . \tag{I.2}$$

This suggests that a convenient representation of the data is given by the local powers,

$$N_{eff} = - p_T^2 \frac{\partial}{\partial p_T^2} \ln(E \frac{d\sigma}{d^3p}) \Big|_{\epsilon \text{ fixed}} \tag{I.3a}$$

and

$$F_{eff} = \epsilon \frac{\partial}{\partial \epsilon} \ln (E \frac{d\sigma}{d^3p}) \Big|_{p_T \text{ fixed}} \tag{I.3b}$$

In power-law models, the deviation of N_{eff} and F_{eff} from their naive constant values arises from a number of sources: (a) the presence of more than one term in the sum, (b) finite mass corrections to the p_T^2 behavior, and (c) the sometimes significant variation of $I(x_1, x_2)$. Although the characterization of the data in terms of the parameters N_{eff} and F_{eff} is tailored to the power law models, it will serve as a general description of the data in much the same way as effective Regge trajectories, $\alpha_{eff}(t)$, and residues, $\beta_{eff}(t)$, can be used to display the systematic features of exclusive data.[22]

Let us assume that F_{eff} and N_{eff} are slowly varying as one approaches the exclusive limit, $\epsilon \to 0$ at large p_T^2 or at fixed angles. The requirement of a

smooth connection[23] between inclusive and exclusive scattering then implies that the associated exclusive process has the behavior (see IV. 12)

$$\frac{d\sigma}{dt} \sim s^{-(1 + N_{eff} + F_{eff})} f(\theta_1, \ldots) \quad . \tag{I.4}$$

In most power law models, $(N + F + 1)_{eff}$ increases as the number of particles involved in the exclusive reaction increases. Hence the value of $(N + F + 1)_{eff}$ yields information on the underlying interaction mechanism responsible for the production of a given particle type in a given kinematic region.

II. THE EFFECTIVE POWER ANALYSIS

Let us now turn to an examination of the existing large p_T data for various types of particles produced in proton-nucleon collisions. Even though it would be useful to carry out analyses at all angles, the only sufficiently complete body of data useful for our purposes was taken in the vicinity of 90° in the center of mass. These consist of π^o data from the Columbia-CERN-Rockefeller (CCR)[16] collaboration and charged particle data from the British-Scandinavian (BS)[17] collaboration (at ISR energies $\sqrt{s} = 23.5$ to 52.4 GeV), and finally the comprehensive charged data of the Chicago-Princeton (CP)[18] collaboration at FNAL energies ($\sqrt{s} = 19.4$ to 27.4 GeV) for protons on heavy nuclear targets. Our analysis will emphasize the observed dynamical differences between production cross sections for different particle types.

Before proceeding with the effective power analysis, we wish to emphasize that there are a number of complications inherent to the CP data. These include

(a) corrections for nuclear target effects[24] in the CP data. The measured A dependence of the π^- production cross sections varies from $A^{0.9}$ to $A^{1.1}$ as p_T ranges from 1 to ≥ 3 GeV/c whereas for proton production the A dependence appears to saturate at $A^{1.2}$ for $p_T \gtrsim 4$ GeV/c. The measured effect for K mesons is similar to that for the pions and $\bar{p}$'s are similar to protons. We have assumed that the above effective A powers depend only on p_T in order to extract the effective per nucleon cross sections from the Tungsten data for each particle type. Furthermore,

(b) the nuclear Fermi motion affects the kinematics so as to increase the average energy in the collision by $\sqrt{s} \rightarrow \sqrt{s}(1 + \frac{1}{2} P_F/M)$, where P_F is a measure of the Fermi momentum. Since the cross section is an increasing function of energy, the fractional error in the extracted F value is

$$\delta F/F = -(1-\epsilon)\epsilon^{-2}(F-1)(P_F^2/4M^2) \qquad \text{(II. 1)}$$

For $P_F \sim M/10$, this is at most a 5% correction in the worst case, $F \sim 10$. The effects of the transverse motion are substantially smaller.

(c) Our analysis corrects kinematically for the fact that data for the CP energies was not taken at precisely 90° in the CM by noting that $\epsilon \equiv \mathcal{M}^2/s = 1 - x_T \csc\theta$. This is the only correction required if the θ dependence of $I(\theta)$ in Eq. (I. 2) is negligible. This is the case for most hard scattering models in the vicinity of 90°.

Because of the above uncertainties, in particular (a), and possible systematic errors between energies, any detailed conclusions based upon the present data must be regarded as somewhat tentative.

We now proceed to extract the two effective power parameters, N_{eff} and F_{eff}, defined in (I. 3). The values of F_{eff} are obtained by using data at different energies but with the same p_T value whereas the N_{eff} extraction requires data at fixed ϵ for different energies. Typically a (logarithmic) interpolation in p_T of the cross section at each energy is required for the latter. This mapping of the data replaces a cross section which varies over ten decades by slowly varying parameters F_{eff} and N_{eff} which can be sensitively compared to the predictions of any theory. In contrast, fits to the data can often achieve reasonable χ^2 values despite systematically incorrect F_{eff} and N_{eff} behavior. Ideally, the extraction of N_{eff} and F_{eff} requires a series of closely spaced energy values. Instead we have, for charged particles, only three FNAL energies ($\sqrt{s} = 19.4$, 23.8, 27.4 GeV) and three ISR energies ($\sqrt{s} = 30.6$, 44.8, 52.7 GeV) while for $p + p \rightarrow \pi^o + X$ we have $\sqrt{s} = 23.5$, 30.6, 44.8, 52.7, and 62.4 GeV. Unfortunately we have had to discard the 62.4 GeV data as being essentially useless for

our purposes because of its large statistical errors. The data from each experiment must be analyzed independently in order to avoid difficulties with relative normalizations which can induce anomalous N_{eff} and F_{eff} values.

For each pair of energies, at fixed p_T, we calculate $(\Sigma \equiv E \frac{d\sigma}{d^3p})$

$$F_{eff} = \frac{\ln[\Sigma(p_T, s_1)/\Sigma(p_T, s_2)]}{\ln[\epsilon(p_T, s_1, \theta_1)/\epsilon(p_T, s_2, \theta_2)]}, \tag{II. 2}$$

while, at fixed ϵ,

$$N_{eff} = -\frac{\ln[\Sigma(\epsilon, s_1)/\Sigma(\epsilon, s_2)]}{2\ln[\sqrt{s_1}\sin\theta_1/\sqrt{s_2}\sin\theta_2]} . \tag{II. 3}$$

In general, N_{eff} and F_{eff} can both be energy dependent. A further advantage of analyzing the ISR and FNAL data separately is that any strong energy dependence of N_{eff} and/or F_{eff} will be most pronounced in the comparison between the two. However, in light of the present statistical errors and the limited number of energies from a given experiment, a too detailed examination of energy dependence within a particular experiment's data is not warranted.

It is perhaps useful to display the sensitivity of N_{eff} and F_{eff} to the statistical errors in more detail. The percentage errors in N_{eff} and F_{eff} are approximately given by

$$\frac{\delta N_{eff}}{N_{eff}} = \left[\frac{\delta\Sigma_1}{\Sigma_1} + \frac{\delta\Sigma_2}{\Sigma_2}\right] / \ln(\Sigma_1/\Sigma_2)\Big|_{\epsilon} \tag{II. 4}$$

and

$$\frac{\delta F_{eff}}{F_{eff}} = \left[\frac{\delta\Sigma_1}{\Sigma_1} + \frac{\delta\Sigma_2}{\Sigma_2}\right] / \ln(\Sigma_1/\Sigma_2)\Big|_{p_T} \tag{II. 5}$$

This error is particularly large for moderate p_T ISR data, where the cross section ratio (Σ_1/Σ_2) is quite near 1. Thus we should not be surprised to observe large fluctuations in the F_{eff} extracted at ISR energies. Even though it is in a region of less sensitivity, some of the CP data points are clearly not of adequate statistical quality to yield meaningful constraints of N_{eff} and F_{eff}. We discard those points for which error bars are of the order of the difference between cross section of two neighboring energies. This limits, primarily, the available $\bar{p}$ and K^- data at the larger p_T values.

The results are presented in Figs. 2 and 3. For the FNAL data x's indicate extractions using the "low" energy pair ($\sqrt{s}$ = 19.4 and 23.8 GeV), and ●'s those for the high energy pair ($\sqrt{s}$ = 23.8 and 27.4 GeV). The discrepancies between the two extractions are some measure of the errors involved as well as possible energy trends. The average value should be somewhat more reliable. The corresponding notation for the ISR data is O for the pair $\sqrt{s}$ = 23.5 - 30.6 GeV, ▲ for 30.6 - 44.8 GeV, and ■ for 44.8 - 52.7 GeV. Note that statistical errors are not shown, but are usually of the same size as the discrepancies from the different energy pairs.

$\underline{\pi^0}$: Fig. 2a shows the N_{eff} for π^0 CCR data. Clearly $N_{eff} \sim 4$ over the entire available x_T range.[25] Fig. 2b shows the corresponding F_{eff} values. The average result is $F_{eff} \sim 11$ though clearly large fluctuations (due presumably to the sensitivity to experimental errors in the small x_T region) about this central value occur.

$\underline{\pi^\pm}$: Fig. 3 gives N_{eff} and F_{eff} for charged hadron production. Note that on each graph two sets of points appear; those for B.S.-ISR (concentrated at low x_T in the N_{eff} graph) and those for the CP-FNAL data. Despite the smooth rise of N_{eff} from 3.5 to 6 over the entire range of data for π^+ and π^- production,

it is clear from the F_{eff} plot that the BS and CP data are quite different, the former having a much higher F_{eff} (more or less consistent with the average value $F_{eff} \sim 11$ of CCR) than the latter at the small p_T values where overlapping F_{eff} extraction is possible. Note, however, that as p_T increases for the FNAL data, F_{eff} rises slowly. The π^- data is quite similar.

$\underline{K^{\pm}}$: The K^+ data is quite similar to the pion data with the exception that the ISR N_{eff} values are about 1/2 unit below those for the pions. In contrast, the K^- data (though limited and not very self-consistent) appears to have a similar N_{eff} to the K^+ but a quite different F_{eff} behavior from the other mesons. F_{eff} is more or less constant throughout the FNAL regime and has a value substantially larger than that for π^+, π^-, and K^+ (except at the highest p_T values). The ISR extractions may also be suggesting a slightly higher F_{eff} for K^- at ISR energies than for K^+, π^+, and π^-.

$\underline{p,\bar{p}}$: The extractions for the proton are seen to be quite different from the meson results. N_{eff} rises from ~ 4 (ISR region) to 8 (FNAL region - high x_T). F_{eff} is again larger for the ISR energies than for the FNAL energies. As in the case of $\pi^{\pm}$ and K^+'s, as p_T increases over the FNAL range, F_{eff} rises from quite a low value to ~ 5 at $p_T \sim 7$ GeV/c. F_{eff} in the ISR region is apparently lower than for the meson data. The N_{eff} behavior for antiproton production appears quite similar to that for protons, but the F_{eff} values are quite different. In the FNAL regime F_{eff} is flat as a function of p_T, large (≈ 8 or 9), and seems to be even higher for ISR energies $\approx 12 - 14$.

Before turning to more detailed considerations we give in Table I the values of $F_{eff} + N_{eff} + 1$ for the CP and BS data. As stated earlier, the sum $(F_{eff} + N_{eff} + 1)$ represents, at least roughly, the overall energy dependence of an associated exclusive limit process which scales as (I.4). From Table I we

see that different particle types yield distinctly different results; the observed ordering agrees with what is expected in models, like the CIM, which associate exclusive processes for $\bar{p}$ and K^- production with higher quark number, and hence stronger energy damping.

TABLE I

APPROXIMATE VALUES OF $(1 + F_{eff} + N_{eff})$

	π^0	π^+	π^-	K^+	K^-	p	$\bar{p}$
CP-FNAL							
$p_T \sim 5 - 6$ GeV	-	12.5	12.5	12.5	14	13	17
$\epsilon = 1 - x_T \sim .5$							
BS-CCR-ISR							
$p_T \sim 3$ GeV	16	14.5	15.5	14.5	16	12	18
$\epsilon = 1 - x_T \sim .87$							

These values are obtained from Figs. 2 and 3, and are uncertain by at least ±1.

III. OTHER THEORIES

One may reasonably ask whether the above results are able to discriminate against any of the various models proposed for high p_T phenomenology. Although an exhaustive discussion of all possible models is beyond the aims of this note, we will at least briefly describe a representative sample of quite different models. The principal experimental feature which any given model must reproduce is the differences in F_{eff} and N_{eff} between the various types of produced particles, i.e., the strong quantum number dependence of the cross sections. Other dynamical features which must be explained are the energy and momentum dependence of F_{eff} and N_{eff}, and, finally, the limiting values of these two quantities in different kinematic regimes.

Hydrodynamical and Thermodynamic Models[14]

These models tend to obtain similar F_{eff}'s for particle and antiparticle at all p_T in apparent conflict with the data. At large p_T, universal, particle-independent, values of F_{eff} and N_{eff} are predicted, because there is no memory of the initial state quantum numbers and all particles have the same temperature. Even allowing for different temperatures, there are more detailed dynamical difficulties. For example, these models suggest that

$$E\frac{d\sigma}{d^3p} \sim \exp\left(- a p_T s^{-h}\right) , \qquad \text{(III. 1)}$$

yielding

$$N_{eff} = \frac{a}{4}(1 - 2h)\, x_T\, s^{\frac{1}{2}-h} . \qquad \text{(III. 2)}$$

Popular values of h, such as $h = 1/8$ (Ref. 26) or $h = 1/4$ (Ref. 27), yield a very strong systematic energy dependence at fixed x_T which is contrary to the data. For example, N_{eff} should change by $\sim$ 30% over the FNAL energy range for $h = 1/8$.

Multiperipheral Models

Two immediate difficulties of the simplest versions of such models (Ref. 28) are that they predict the same F_{eff} and N_{eff} for particles and antiparticles and that the pion and kaon cross sections should have the same form except for mass-dependent effects (Ref. 29) that should be small at the larger p_T values. Although these models can naturally yield an $N_{eff} \sim 4$ (for example by assuming an underlying ϕ^3 theory), they have considerable difficulty in understanding the higher N_{eff} values appropriate to the FNAL data. The data can perhaps be interpreted in terms of generalized versions of the above models which incorporate quantum number dependence in trajectories and more general energy dependence.

Quark-Quark Scattering[2,19]

The first and most obvious difficulty of this approach is the natural expectation $N_{eff} = 2$ for scale-invariant quark-quark scattering is considerably below that appropriate to any present data. Regardless of the assumed energy dependence of the basic scattering process, all such models have systematic difficulties with particle ratios since a universal N_{eff} is predicted. Furthermore, in the absence of "leading particle" diagrams, F_{eff} for pions should be lower than that for protons at any given p. This, too, is contrary to the data.[30] Natural modifications of the naive quark-quark scattering form can arise in asymptotically free gauge theories. One proposal is that the cross section should have the form[31]

$$E \frac{d\sigma}{d^3p} \propto \frac{\epsilon^{F + a \ln \ln (p_T^2/\mu^2)}}{p_T^4 \ln (p_T^2/\mu^2)} \qquad \text{(III. 3)}$$

implying

$$F_{eff} \sim F + a \ln \ln(p_T^2/\mu^2) \qquad \text{(III. 4)}$$

independent of energy. Even though the overall magnitude of N_{eff} ($\approx 2 + a/\ln p_T^2$) is improved, the predicted energy independence of it and F_{eff} in going from ISR to FNAL energies is a difficulty for this approach. Another possibility is that the scale invariant interaction itself is modified by neutral vector mesons or gluons in a gauge theory. The form suggested by Fried et al.[15] is

$$E \frac{d\sigma}{d^3p} = G(x_T)\, s^{-n} \qquad \text{(III. 5)}$$

$$n \cong 2 + 4\gamma x_T \ .$$

While the extracted N_{eff} values could be consistent with the predicted dependence (provided γ is particle dependent) the FNAL meson data yield N_{eff}'s which change very slowly at high x_T. In addition F_{eff} is predicted to be energy independent (since G is) at fixed p_T. This, again, appears to be in conflict with the transition between ISR and FNAL data.

A common difficulty of many of the above approaches is the assumption of a single contributing subprocess so that the cross section is dominated by one term. While the use of more than one subprocess will not solve all the difficulties of the above approaches, it is clear that this type of freedom is essential to describe the experimental results - in particular the difference between ISR and FNAL energies.

IV. CIM THEORY

In order to present a meaningful analysis of the data within the framework of the constituent interchange model, we will present in this section a review of the essential features of this approach to large p_T phenomena. Within the framework of hard scattering models there are a great number of possible candidates for the underlying large p_T subprocesses. It is thus necessary to systematize the calculational rules in order to present a simple confrontation with the data. The primary ingredient is the use of dimensional counting[5,6] which has already been shown to be successful in describing the experimental features of fixed angle two-body scattering processes. To review briefly, since any two-body reaction $a + b \to c + d$ has fixed angle behavior of the form

$$\frac{d\sigma}{dt}(a + b \to c + d) \sim s^{-[n_a+n_b+n_c+n_d-2]} f(t/s) \quad , \tag{IV.1}$$

the inclusive cross section Eq. (I.1) behaves as

$$E\frac{d\sigma}{d^3p} \equiv \sum_{abcd} (p_T^2 + M^2(abcd))^{-N} f(\theta_{c.m.}, \epsilon) \; , \tag{IV.2}$$

where

$$N = n_a + n_b + n_c + n_d - 2 \tag{IV.3}$$

and $M_{(abcd)}$ is a mass characteristic of the subprocess. Here n_H is the number of quarks in hadron H. More generally $N + 2 = n_{active}$ is the number of elementary fields (lepton–photon–quark) participating in the large angle subprocess. Thus for electron-quark or photon-quark or quark-quark scattering ($n_{active} = 4$) one obtains the standard scale-invariant p_T^{-4} predictions of the parton model. Quark-meson scattering ($n_{active} = 6$) gives the CIM prediction of p_T^{-8}. Other quark-hadron or hadron-hadron reactions yield p_T^{-8}, p_T^{-12}, p_T^{-16} ... as more and more elementary fields are involved in the large p_T reaction.

Physically, one pays the "penalty" in the cross section of a factor p_T^{-4} for changing the direction of each additional quark or lepton line. Note that these quark counting rules automatically incorporate the predictions of asymptotic dipole baryon and monopole meson form factors. They are derived assuming a basic scale-invariance of the scattering amplitude at short distance (as in characteristic of simple Born graphs in renormalizable perturbation theory) and assuming that the hadronic Bethe-Salpeter wave function is finite (corresponding to limited binding corrections). One can extend the predictions to allow for logarithmic modifications of the scaling laws or small anomalous dimensions, but we shall not find this necessary here.

Besides the counting rules for the subprocess fixed angle energy dependence, one is fortunate in also having closely related constraints on the distribution functions $G_{a/A}(x)$. These are obtained by assuming, as before, an underlying scale-invariant theory; it is easy to show that for $x \to 1$ [9]

$$G_{a/A}(x) \sim (1-x)^{2n(\bar{a}A)-1} , \tag{IV.4}$$

where $n(\bar{a}A)$ is the number of quarks in the state $\bar{a} + A$; i.e., the number of quarks "left behind". Some typical cases are

$$G_{q/p} \sim (1-x)^3 , \quad G_{\bar{q}/p} \sim (1-x)^7 , \quad G_{q/\pi} \sim (1-x) . \tag{IV.5}$$

All these results are consistent with the generalized form factor behavior

$$F_{a/A}(t) \sim t^{-n(\bar{a}A)} \tag{IV.6}$$

and the analogue of the Drell-Yan-West relation for νW_2.

The prediction $\nu W_2^{\bar{q}} \sim (1-x)^7$ for antiquarks in the nucleon has been used to great advantage in Refs. 32 for the parametrization of the parton distributions obtained from neutrino and electron deep inelastic scattering. It is, however, evident that one must take $G_{d/p}(x) \sim (1-x)^4$ for the down-quark

distribution in the proton and up-quark distribution in the neutron in order to parametrize the observed behavior of $\nu W_2^p/\nu W_2^n$. This indicates strongly that a simple symmetrical three-quark model for the nucleon is too naive. The applications to the FNAL data discussed in this paper, however, are not sensitive to this modification, because of the nuclear target.

Using Eq. (IV.4) we also have $(M = \pi, K^-, \rho, \ldots)$

$$G_{M/p} \sim (1-x)^5, \quad G_{K^-/p} \sim (1-x)^7, \quad G_{\bar{p}/M} \sim (1-x)^5, \quad G_{\bar{p}/p} \sim (1-x)^{11} \tag{IV.7}$$

Some consequences of these results for inclusive reactions in the triple Regge region are discussed in Ref. 9. Note also the mild falloff of $G_{(qq)/p} \sim (1-x)$ reflecting the ability of the diquark system to carry off a large fraction of the nucleon momentum (only one quark has to be stopped).

Applying the result (IV.4) to Eq. (I.1) we immediately obtain the convenient counting rule (as $\epsilon \to 0$)

$$E\frac{d\sigma}{d^3p} \sim \sum_{abcd} (p_T^2)^{2-n_{active}} \epsilon^F f(\theta_{c.m.}) , \tag{IV.8}$$

where F, the degree of "forbiddenness", is given by[9]

$$F = 2\, n_{passive} - 1 \tag{IV.9}$$

and where, for hadronic reactions,

$$n_{passive} = n(\bar{a}A) + n(\bar{b}B) + n(\bar{C}c) \tag{IV.10}$$

is the number of passive spectators in the reaction. One can readily check that this rule is consistent with the Bjorken-Kogut correspondence principle,[23] crossing properties,[33] and normal parton model predictions for lepton-hadron processes, such as $pp \to \mu X$. In the case of electromagnetic couplings, we

have the further rule that

$$F = 2\, n^{\text{hadronic}}_{\text{passive}} + n^{\text{e.m.}}_{\text{passive}} - 1 \,, \tag{IV.11}$$

where $n^{\text{e.m.}}_{\text{passive}}$ is the number of spectator quarks or leptons arising from a point electromagnetic coupling. Note that photons are not counted in the spectator rule. Accordingly, spin-one gluons which have an elementary coupling to quarks never affect the $\epsilon \to 0$ end point behavior or probability distributions to finite order in perturbation theory. The difference in counting emerges as a result of the point-like nature of electromagnetic interactions.[34] This rule applies to ordinary radiative processes and radiative corrections (in which case there is an extra factor of $(\log s/m_e^2)$ for each electromagnetically radiated particle) as well as to photoinduced processes. The counting rules correspond to the intuition that as the number of spectators increases there is less available phase-space and the power of ϵ increases.

As a final constraint and classification tool, we shall use the correspondence principle of Bjorken and Kogut,[23] which requires a smooth connection between the form of the inclusive cross section for $\epsilon = \mathcal{M}^2/s \to 0$ and a corresponding exclusive cross section. This connection, the generalization of Bloom-Gilman duality for deep inelastic lepton scattering, can be proven in theories of the type considered as was mentioned above. Thus, if a contribution to the inclusive cross section for $A + B \to C + X$ at fixed $\theta_{\text{c.m.}}$ is to join smoothly for $\epsilon \to 0$ to an exclusive cross section for $A + B \to C + D + \ldots E$, we then have[23]

$$\int^{M^2} d\mathcal{M}^2 \frac{d\sigma}{dt\, d\mathcal{M}^2} (A + B \to C + X) \simeq \int^{M^2} \frac{1}{\pi} \frac{d\mathcal{M}^2}{s} \frac{\epsilon^F}{(p_T^2)^N} f^{\text{incl}}(\theta)$$

$$\simeq \frac{1}{s^{N_{excl}}} f^{excl}_{A+B\to C+D+\ldots E}(\theta_1,\ldots) \qquad \text{(IV.12)}$$

where

$$N = n_a + n_b + n_c + n_d - 2 \qquad \text{(IV.13)}$$

and

$$N_{excl} = N + 2n_{passive} = 1 + N + F\,. \qquad \text{(IV.14)}$$

It is apparent that in this exclusive limit the total number of active quarks (since all are active) is, in fact, $N + 2n_{passive} + 2$, so that the power, N_{excl}, conforms to dimensional counting. The angular functions f^{excl} and f^{incl} are similarly and internally related.

Note further that all of the contributions which yield the same N_{excl}, i.e., are dual to the same exclusive channel, may be summed in the form[9]

$$\sim \frac{\epsilon^F}{(p_T^2)^N}\left[1 + O\left(\frac{M^2}{p_T^2\epsilon}\right)^2 + \ldots + O\left(\frac{M^2}{p_T^2\epsilon}\right)^{F+1}\right] , \qquad \text{(IV.15)}$$

where the first term clearly dominates for $p_T^2 >> M^2$, and the subsequent terms correspond to allowing the passive spectator quarks to become active large momentum transfer participants. The last term gives the exclusive channel limit. Note that the corrections to the leading term are of the same form as that obtained by using

$$(p_T^2)^{-N}\,\epsilon^{-1}\,(\epsilon')^{F+1}$$

where $\epsilon'^2 = \epsilon^2 + O(M^4/p_T^4)$, and are analogous to the corrections from using the Bloom-Gilman variable ω' rather than ω in the analysis of deep-inelastic scattering. The calculation of the cross section normalization is very difficult in this limit since the various terms become coherent in this limit.

Thus, hard scattering model predictions for particle ratios at large p_T, Eq. (II. 2), can be summarized as follows: For the <u>same</u> p_T power law (p_T^{-4}, p_T^{-8}, or p_T^{-12}, ...), the cross section for production of particle type C as compared to type C' is given by

$$\frac{E\,\frac{d\sigma}{d^3p}\,(A + B \to C + X)}{E\,\frac{d\sigma}{d^3p}\,(A + B \to C' + X)} \sim \epsilon^{N_E(C)-N_E(C')}\,, \tag{IV. 16}$$

where, at 90°, $\epsilon = 1 - X_T$. Here $N_E(C)$ is the dimensionally determined power falloff at fixed angle of the cross section for the first exclusive contributing channel (i.e., with fewest elementary quarks) which contains particle C plus other nonexotic hadrons, and originates from A + B. The corresponding form for $E\,\frac{d\sigma}{d^3p}$ for a given value of $N_E(C)$ is

$$E\,\frac{d\sigma}{d^3p}\,(A + B \to C + X) \sim \frac{I_4}{p_T^8}\,\epsilon^{N_E(C)-5} + \frac{I_6}{p_T^{12}}\,\epsilon^{N_E(C)-7} + \ldots \tag{IV. 17}$$

These statements assume that all possible relevant subprocesses are significant. However, certain of these subprocesses may not be allowed by a specific model. For example, in the CIM, in which the contributing hard interactions must all be derived from quark interchange or exchange among hadrons, the p_T^{-4} terms which arise only from quark-quark scattering are absent. The reaction q + (qq) $\to$ q + (qq) is also not allowed in the CIM, but it is present in Preparata's massive quark model.[10] Conversely, assumptions which are too restrictive can be inconsistent with crossing to the process $\bar{C} + B \to \bar{A} + X$; this is the case if one assumes absolute dominance of annihilation processes such as $q + \bar{q} \to M + \bar{M}$, for example.[25]

Let us now turn to a more detailed discussion of the contributions present in the CIM. Given the absence of any quark-quark scattering terms (as first predicted on the basis of a study of the angular dependence of elastic scattering), the leading contributions then arise from terms with six active quarks and have $N = 4$.

Thus the limiting behavior at fixed ϵ and angle for any hadronic production process will be p_T^{-8}. However, it is equally clear that as ϵ becomes small, terms with larger N, p_T^{-12}, p_T^{-16}, . . . , which in general can have smaller values of F, will become increasingly important. As we shall see in the next section, the above expectations are consistent with the available data. In particular, the p_T^{-8} behavior does seem to emerge at ISR energies.

The allowed subprocesses in the CIM for the lowest three values of N are listed in Table II. For each subprocess, the minimal F value for the production of a given particle type is given for proton-nucleon collisions.[36]

TABLE II

CIM SUBPROCESSES

		F_{min} for (pp →)			
	Subprocess	$\pi^{\pm,0}, K^+, \rho^{\pm,0}$	K^-	p	$\bar{p}$
N = 4	$q+M \to q+M$	9	13	13	15
	$q+\bar{q} \to M+\bar{M}$	11	11	17	17
	$q+q \to B+\bar{q}$	9	9	7	11
N = 6	$q+(qq) \to M+B$	5	9	5	11
	$q+B \to q+B$	5	9	3	11
	$M+M \to M+M$	11	11	17	17
	$q+\bar{q} \to B+\bar{B}$	17	17	11	11
N = 8	$(qq)+B \to (qq)+B$	7	11	1	11
	$M+B \to M+B$	5	9	5	11

In general, subprocesses which are related by crossing to those listed in the table, such as $M+\overline{M} \rightarrow q+\bar{q}$, also are to be included, but these yield higher F values and thus are nonleading contributions in the $\epsilon \rightarrow 0$ limit for proton-proton scattering.

The CIM postulate, which allows only subprocesses involving at least one hadron, is natural from the point of view of containment or bag models in which the direct quark-quark interaction can be made small without affecting the quark-container interaction. Additionally, the CIM can be regarded as a dynamical prescription for calculating duality diagrams.

Within the CIM framework, proton production is a somewhat special case. First, there is no minimal $F = 5$, $N = 4$ subprocess. Second, the subprocess $q+q \rightarrow B+\bar{q}$ is not necessarily present. It is intimately related to the basic wave function of the baryon. This term would be absent in theories in which the baryon is a bound state of a quark plus a strongly bound diquark core. This is a striking example of how large p_T experiments may be able to resolve an essential feature of the short distance structure of baryons.

While the above N and minimal F values appropriate to a given subprocess describe the dominant kinematic variations for sufficiently small ϵ and large p_T, there are corrections to both as one moves away from this region. In the case of N_{eff}, the corrections are relatively simple. They take the form of mass corrections to p_T^2. As outlined earlier, a given subprocess is assumed to have the form $(p_T^2 + M^2)^{-N}$ and hence the local N_{eff} is

$$N_{eff} = N(1 + M^2/p_T^2)^{-1} \qquad \text{(IV.18)}$$

Local exponents appropriate to $N = 4$ and 6 are shown as a function of x_T for two energies (ISR and FNAL) and several M^2 values in Fig. 4. These can be used

as a tableau to directly compare with the extracted N_{eff}'s and to estimate the mass values appropriate to a given reaction. Another modification, which is important at quite small p_T^2, arises because of moving trajectories.[3,7,9] The power N is related to the asymptotic value $\alpha(t' \to -\infty)$ of the Regge trajectory of the subprocess $\frac{d\sigma}{dt'}(a + b \to c + d)$. When $|t'| \lesssim 2\ \mathrm{GeV}^2$, $\alpha(t')$ rises toward positive values and N is correspondingly decreased. The effect is difficult to distinguish from the M^2 effects for the $p_T > 2$ GeV/c data analyzed here.

V. THE PHYSICS OF F_{eff}

Although the limiting value of N_{eff} has direct physical significance, its shape is determined mostly by essentially kinematic mass corrections. This is definitely not the case for the shape of the F_{eff} curve, which can directly reflect the constituent nature of the hadrons involved. In this regard it is important to note that mass corrections to ϵ are of the order M^2/s and hence are generally small. Thus it is the detailed shape of the overall probability functions which will significantly modify the naive minimal F values when ϵ is not small.

Since a typical distribution function appearing in the convolution integral, Eq. (I. 1), may be expected to display a peaking or at least a plateau as is the case for the deep inelastic structure functions, it follows that the inclusive cross section should display a corresponding smeared quasielastic peak or plateau. Such behavior can be thought of as arising from several distinct sources. The first effect is that the minimal F values arise from processes with the minimum number of spectators. Quite often this means that the associated term is far from Feynman scaling, since it involves a minimum quark configuration whose wave function does not have Regge behavior. Therefore, background terms arising from high wave function components (involving more spectators) which lead to larger F values must eventually become dominant in order to achieve Feynman scaling as $\epsilon \rightarrow 1$.

The next complication is that for probability functions of a given shape the convolution integral and the angular distribution of the given subprocess can introduce additional variation of F_{eff} at finite ϵ.

In order to discuss more fully these effects, it will be convenient to write the convolution integral, Eq. (I. 1), in the following form:[37]

$$E\frac{d\sigma}{d^3p} = \frac{2}{\pi}\int_{-(1-2x_1)}^{(1-2x_2)} \frac{dz}{1-z^2}\, F_{a/A}\left(\frac{2x_1}{1+z}\right) F_{b/B}\left(\frac{2x_2}{1-z}\right)\frac{d\sigma}{dt}\left(s' = \frac{4p_T^2}{1-z^2}\,,\ z\right) \qquad (V.1)$$

where z is the cosine of the scattering angle in the c.m. of the subprocess and $F(y) = yG(y)$. This result can be readily extended to allow for fragmentation of c into C using Eq. (I.1).

In a moment we will discuss the limiting behaviors of Eq. (V.1) and the resulting predictions for F_{eff}. First, let us consider the simple case when the distributions are peaked at their natural momentum fraction: $G_{a/A}(x) = \delta(x - n_a/n_A)$, $G_{b/B}(x) = \delta(x - n_b/n_B)$; here $n_A = n_a + n(\bar{a}A)$ and $n_B = n_b + n(\bar{b}B)$ are the total number of available quarks in the projectile and target, respectively. Note that this is the <u>exact</u> distribution in the limit of <u>zero</u> binding. For the peaked distributions, we must have

$$z = \frac{n_A}{n_a}x_1 - \frac{n_B}{n_b}x_2 \qquad (V.2)$$

and

$$1 = \frac{n_A}{n_a}x_1 + \frac{n_B}{n_b}x_2 \qquad (V.3)$$

Thus we expect that for detection at 90° the cross sections will have a quasi-elastic peak at the value

$$x_T = \hat{x}_T \equiv \frac{2}{\frac{n_B}{n_b} + \frac{n_A}{n_a}}\,, \qquad (V.4)$$

and be spread out around this value by the effects of finite binding. At the peak, the derivative with respect to x_T vanishes, and hence F_{eff} should vanish also at this point. (Note that $\hat{x}_T$ is multiplied by $n_C/(n_C + n_{\bar{C}c})$ if final state

bremsstrahlung occurs.) Note also that the center-of-mass angle of the recoil system d in the active process $a + b \rightarrow c + d$ peaks at

$$\tan \hat{\theta}_d = \frac{\hat{x}_T}{\frac{n_b}{n_B} - \frac{n_a}{n_A}} \tag{V.5}$$

The actual physical distributions which must be used in Eq. (V.1) can be expected to have a relatively complicated behavior, but for simplicity they may be characterized as a sum of terms of the form

$$G(y) = \frac{F(y)}{y} = G\, y^h (1-y)^g \quad . \tag{V.6}$$

The endpoint behavior at $y = 0$ and $y = 1$ can be established: For $G_{a/A}(y)$, we have $g = \gamma n(\bar{a}A)-1$, where $n(\bar{a}A)$ is the number of spectators, as discussed earlier. [The value of γ is 2 for quark-spectators bound in hadrons, 1 for elementarily coupled leptons.] The value of h depends on the type of wave function component being considered. For a single "valence" type wave function, i.e., a state containing a finite number of particles, h is $\gamma n_a - 1$. This ensures the correct wave function normalization and that $\langle x_a \rangle = n_a/[n_a + n(\bar{a}A)] = n_a/n_A$. On the other hand, we also know that the physical distributions at $y \rightarrow 0$ are related to the high energy behavior of the forward $\bar{a}A$ amplitude: Pomeron and Regge behavior require $h = -\alpha < 0$. Specifically, for a Pomeron-behaved sea component, $h = -1$, corresponding to the Feynman dx/x distribution; Reggeon components have $h \sim -1/2$. Accordingly, the Pomeron and Regge terms must be interpreted as a coherent superposition of states with an arbitrary number of spectators.[38] We emphasize that the separation of the physical distributions into Pomeron, Regge, and valence components of the form of Eq. (V.6) should be regarded as a convenient idealization of a more complicated situation.

Writing the differential cross section for the subprocess as

$$\frac{d\sigma}{dt} = s'^{-N}\left(\frac{1-z}{2}\right)^{-T}\left(\frac{1+z}{2}\right)^{-U} \tag{V.7}$$

and introducing probability functions of the form (V.6) the convolution integral becomes

$$E\frac{d\sigma}{d^3p} \simeq (p_T^2)^{-N}\,\epsilon^F\, x_1^{r_A}\, x_2^{r_B}\, J(x_1,x_2) \tag{V.8}$$

where

$$J(x_1,x_2) = J_0\int_0^1 d\eta\;\eta^{g_A}(1-\eta)^{g_B}(x_1+\epsilon\eta)^{N_A}(x_2+\epsilon(1-\eta))^{N_B}\,, \tag{V.9}$$

$$N_A = N - 1 - g_A - r_A - U\,,$$

$$N_B = N - 1 - g_B - r_B - T\,,$$

$$F = 1 + g_A + g_B = 2n(\bar{a}A) + 2n(\bar{b}B) - 1\,,$$

$$r_A = h_A + 1,\quad r_B = h_B + 1\,,$$

and recall that at 90°, $x_1 = x_2 = x_T/2$.

The effect of the η-integral is usually to increase F_{eff} for $\epsilon \sim 1$, whereas the explicit powers of x_1 and x_2 outside the integral tend to decrease the effective F value as ϵ increases. At 90°, the F_{eff} for a contribution of the above form is

$$F_{eff} = F - \frac{\epsilon}{1-\epsilon}(r_A+r_B) + \epsilon\frac{\partial}{\partial\epsilon}\ln J \tag{V.10}$$

where in the limit $\epsilon = 1$,

$$\epsilon\frac{\partial}{\partial\epsilon}\ln J\Big|_{\epsilon=1} = \frac{1}{2}N_A\left(1 - \frac{1+N_B+g_B}{N_A+g_A}\right) + (A \leftrightarrow B)\,. \tag{V.11}$$

Except for a few cases, this last term's contribution tends to increase F_{eff} for $\epsilon \sim 1$. It is always positive for Feynman-scaling contributions and decreases to zero as $\epsilon \to 0$. Thus the Feynman-scaling contributions monotonically decrease with ϵ, whereas the terms with $r_A + r_B \neq 0$ correspond to a peaked "quasielastic" distribution in ϵ.

As we have noted, the possibility of a vanishing F_{eff} in Eq. (V.10) has an elegant and simple interpretation. Physically, each secondary particle, a or b, carries average momentum in the c.m. frame

$$|\vec{p}_a| \sim \frac{\sqrt{s}}{2} \frac{n_a}{n_a + n(\bar{a}A)} , \quad |\vec{p}_b| \sim \frac{\sqrt{s}}{2} \frac{n_b}{n_b + n(bB)} \tag{V.12}$$

For example, the simple momentum distribution $xG_{a/A}(x) \sim x^{\gamma n_a}(1-x)^{\gamma n(\bar{a}A)-1}$ peaks at $x \sim n_a/(n_a + n(\bar{a}A) - \gamma^{-1})$, which is close to the weak binding value. (This sensible result again motivates the choice $h = \gamma n_a - 1$ for the finite particle wave function.) Thus the most likely kinematical situation consistent with the on-shell constraint $s' + t' + u' = 0$ and a fixed number of spectators are the values of x_1, x_2, and x_T given in Eqs. (V.2-4). In particular, the peak of the inclusive distribution at 90° and the zero of F_{eff} should occur near this value of $\hat{x}_T$. This is the natural extension of the average momentum value for probability distributions: the relative number of active and spectator quarks in each hadron A, B, and C determines the most likely trigger particle x_T value at any given transverse momentum.

Thus the shape of the F_{eff} curve can be physically quite meaningful provided the various components can be at least approximately isolated. Isolation of these components requires use of difference data, sum rules, and other intercomparisons. Some experimental examples will be presented in the next section. Such techniques have been applied with substantial success to separation

of the various components of quark distribution functions from deep inelastic data. In any case, the larger the contributions from Feynman scaling and Regge terms and hence the greater the number of spectators, the smaller the value of x_T at which F_{eff} will pass through zero.

A simplifying device, which was shown to be adequate in the extraction of the quark distributions from deep inelastic data,[39] is to associate two extra spectators ($q\bar{q}$) with the Pomeron (P) and Regge (R) components beyond the minimum number required for the valence (V) component. Here we use this device only to illustrate how F is expected to increase as one gets into the Regge and Pomeron region. Since in the present case two such distributions are being convoluted, we can expect contributions in the general case with the following types of limiting behaviors[40]

$$
\begin{array}{ll}
x_T^{4}\,\epsilon^{F} & \text{(V-V)} \\
x_T^{2+\frac{1}{2}}\,\epsilon^{F+4} & \text{(V-R+R-V)} \\
x_T^{2}\,\epsilon^{F+4} & \text{(V-P+P-V)} \\
x_T\,\epsilon^{F+8} & \text{(R-R)} \\
x_T^{\frac{1}{2}}\,\epsilon^{F+8} & \text{(R-P+P-R)} \\
\epsilon^{F+8} & \text{(P-P)}
\end{array}
\qquad (V.13)
$$

The relative weightings of the P, R, and V terms may be quite different for the quark, antiquark, and hadron distributions. Thus it should be stressed that in general such details of the theory can be checked at this level only by comparing different reactions that involve the same probability functions. Regardless of the modifications to F_{eff} which one may reasonably expect in the region where ϵ

is not small, we emphasize that the ultimate tests of the predictions for F lie in the limiting case of $\epsilon \rightarrow 0$.

VI. EXPERIMENTAL COMPARISON

A comparison of the predictions made in the previous section with experiment will now be made. Let us start by describing a few important overall features. First we note that the CIM quite naturally incorporates the differences between particle types needed to describe the various F_{eff} and N_{eff} extractions. It also incorporates naturally the differences observed between the ISR and FNAL energy ranges. More specifically:

(a) The value of $N_{eff} \sim 4$ for the ISR π^0 data was predicted by the CIM.[7] This confirmation is essential before proceeding further with this model. It is to be expected that this minimum N value should dominate all the moderate p_T ISR meson data and indeed this is consistent with the experimental values for N_{eff} provided the expected mass effects illustrated in Fig. 4 with M^2 of order 1 to 2 GeV^2 are incorporated. Although the experimental errors are considerable, the values of the F_{eff}'s for mesons are relatively large and consistent with the values predicted on the basis of p_T^{-8} subprocesses.

(b) Because of the smaller ϵ values of the FNAL data, subprocesses with smaller F values, and consequently higher N values, should become more important. Indeed, all the FNAL meson data appears to be consistent with the dominance of $(p_T^2 + M^2)^{-6}$ terms. The F_{eff} values are lower than those from the ISR and their limiting values are consistent with expectations.

(c) The p and $\bar{p}$ data are somewhat more complex and clearly show substantial $N_{eff} = 8$ terms in the FNAL energy range. Despite this complexity, the F_{eff} values behave as expected (note the low values for p compared to $\bar{p}$) and a consistent picture can be constructed.

(d) A convenient way of displaying the overall consistency of this approach is to compare the limiting experimental values of $N_{EX} = (F + N + 1)_{eff}$ with the

predictions of various subprocesses in the CIM and in Table III. The general consistency with the data is striking. The predicted ordering $N_{EX}(\bar{p}) > N_{EX}(K^-) > N_{EX}(K^+, \pi) \geq N_{EX}(p)$ is correct, as well as the individual absolute predictions.

TABLE III

PREDICTIONS FOR $N_{EX} = N_{eff} + F_{eff} + 1$
(proton-nucleon collisions)

Produced Particle		$[\pi^{\pm,0}, K^+]$	K^-	p	$\bar{p}$
Minimum Exclusive Channel		12	14	10	16
CIM Subprocesses:					
N=4, p_T^{-8}	$q + q \rightarrow B + \bar{q}$	14	14	12	16
	$q + M \rightarrow q + M$	14	20	18	22
	$\bar{q} + M \rightarrow \bar{q} + M$	16	18	22	20
	$q + \bar{q} \rightarrow M + \bar{M}$	16	16	22	22
ISR (See Table I)		15 ± 1	16 ± 1	12* ± 1	18* ± 1
N=6, p_T^{-12}	$q + 2q \rightarrow B + M$	12	16	12	18
	$q + B \rightarrow q + B$	12	16	10	18
	$\bar{q} + \bar{q} \rightarrow B + \bar{B}$	18	18	18	18
	$M + M \rightarrow M + M$	18	18	18	18
FNAL (See Table I)		12.5 ± 1	14 ± 1	13 ± 1	18 ± 1

* Note that the N_{eff} for p and $\bar{p}$ production at the ISR indicate contributions from N = 6 processes.

(e) Since the $\bar{p}$'s and K^-'s are apt to originate from beam-independent, Feynman scaling distributions, the F_{eff} curves are expected to be much flatter than the primarily valence-derived particles and may possibly even rise as $\epsilon \rightarrow 1$. As discussed in the previous section, the primarily valence-derived particles (P, K^+, $\pi^{\pm,0}$) are expected to have decreasing F_{eff}'s as $\epsilon \rightarrow 1$.

(f) The N_{eff} and F_{eff} obtained from the difference between particle and antiparticle cross sections are particularly interesting. The F_{eff} dependence can directly reflect the quasielastic features of the hard scattering model as discussed in Section V. The F_{eff} analysis for $K^+ - K^-$ and $p-\bar{p}$ is shown in Fig. 5. Although the errors are magnified, F_{eff} actually does vanish for both differences, as expected from the model. The zeros occur at a quite reasonable position, $\hat{x}_T \sim 0.2 - 0.3$ in the FNAL energy range and $\hat{x}_T \sim 0.1 - 0.2$ in the ISR range. These values of $\hat{x}_T$ indicate the typical fraction of center-of-mass hadronic beam energy which is maximally effective in producing large p_T particles. The fact that $\hat{x}_T$ is lower at the higher ISR energies is consistent with the fact that there are more spectators (and higher multiplicity) in the beam and target fragmentation regions for the processes which are important at the ISR compared to the FNAL regime: $F_{eff}(\text{ISR}) > F_{eff}(\text{FNAL})$. The N_{eff} of the difference $K^+ - K^-(p-\bar{p})$ is consistent with that of K^+ or K^- (p or $\bar{p}$) at both ISR and FNAL energies.

There are uncertainties in trying to interpret the experimental values of $\hat{x}_T$ directly in terms of the probability distributions and subprocesses. However, using the framework of Section V, one might be able to proceed as follows. If the $q + qq \rightarrow B + M$ subprocess is dominant for FNAL energies, then the minimum number of spectators is 3 (this is consistent with $F_{eff} \sim 5$ at $\epsilon \sim 0$ for p or K^+ production), and $(\hat{x}_T)_{max} = 4/9$ using Eq. (V.4). However, the Reggeon terms in the distribution are surely important (see Eq. (V.10)) reducing $\hat{x}_T$ to about 1/3 or smaller, corresponding to at least 5 spectators. (See discussion of Eqs. (V.13) and Ref. 38.) Precise checks of the predicted values of x_T will require double and triple difference experiments which can isolate the various components.

Now let us try to understand in more detail the particular subprocesses that dominate the production cross sections of each particle.

$\underline{\pi^0}$: As seen from Fig. 2, a single term of the form $\epsilon^{11}(p_T^2 + M_4^2)^{-4}$ provides a good representation of the CCR data. The fluctuations of F_{eff} are probably due to small errors in the data since Eq. (II.5) yields $\delta F/F \sim 60 - 70\%$ for 10% statistical errors. The M_4^2 parameter is not easily determined from the CCR data which only requires $M_4^2 \lesssim 1.5$. The value $F \sim 11$ is consistent with all the $N = 4$ subprocesses when the possibility of both Feynman scaling and nonscaling terms is taken into account. Correlation measurements will be required to distinguish between the quark-meson scattering and $q\bar{q} \rightarrow M\bar{M}$ annihilation contributions. The rising multiplicity[41] on the side opposite to the π^0 is natural to the $q+M \rightarrow q+M$ process. The observed constancy of the ratio $(\eta^0/\pi^0) = 0.55 \pm 0.11$ (Ref. 42) is consistent with the CIM dynamics and the assumed quark content of these mesons.

$\underline{\pi^\pm}$: The $\pi^\pm$ data of BS and CP clearly show that both $N = 4$ and 6 terms are required. The normalization of the $N = 4$ term is essentially determined by the CCR π^0 data. The dominance of the $N = 6$ term in the CP data is consistent with this normalization because of the difference in F values of the two terms. The $N = 6$ subprocesses with minimal $F(=5)$ are $q + (qq) \rightarrow M + B$ and $B + q \rightarrow B^* + (q) \rightarrow B^* + (q' + M)$. The experimental F_{eff} does seem to be approaching the limiting minimal value of 5. Both subprocesses predict a recoil baryon system on the opposite side (and on the same side if the detected meson arises from the decay of the B^*). The shape of the N_{eff} curve in the two regions suggests masses of $M_4^2(\pi) \sim 1.2\ \mathrm{GeV}^2$ and $M_6^2(\pi) \sim 1.7\ \mathrm{GeV}^2$. The F_{eff} curves for the CP data display the expected behavior. The fact that the F_{eff}'s do not vanish implies that there is a large Feynman-scaling contribution as $\epsilon \sim 1$.

[The near equality of π^+ and π^- at all x_T does not imply complete dominance by Feynman-scaling terms since the valence contributions are nearly symmetric for a nuclear target.] Measurements of the angular dependence of the π^+ and π^- yields - even on a nuclear target - would help separate these terms since the ratio π^+/π^- should increase towards the forward direction.

$\underline{K^\pm}$: The K^+ cross section is very similar to that of $\pi^\pm$ in accord with expectation. The only observable difference besides an overall normalization is that at the lowest x_T values both the BS and CP data have $N_{eff}(K) \simeq N_{eff}(\pi) - 0.5$ for both the K^+ and K^-. This is easily accounted for by slightly larger mass parameters for the K's, namely $M_4^2(K) \sim 2.0\ GeV^2$ and $M_6^2(K) \sim 2.1\ GeV^2$, entirely in accord with one's naive expectations.

In contrast to the near equality of N_{eff} for K^+ and K^-, their respective F_{eff}'s are quite different. For the ISR range, $F_{eff}(K^-)$ is around 14, though a value of 11 cannot be ruled out. This is higher than the value found for pions, and is close to the minimal F appropriate to the $q + M \rightarrow q + M$ process, F = 13 (17 if nonminimal bremsstrahlung). Thus it is very interesting to determine F_{eff} more accurately and to measure correlations in order to distinguish the contributing subprocess. Note that the minimal annihilation process always has a recoiling strange meson opposite to the detected K^-; this is not necessarily the case if one triggers on a K^+. If the minimal $q + M \rightarrow q + M$ subprocess dominates where $M = K^+$ or K^-, then the strangeness is expected to be balanced in the beam fragmentation region.

For the FNAL range, $F_{eff}(K^-)$ is between 7 and 9. In the framework of the CIM, the limiting value of F cannot be less than 9 for N = 6 unless the selection rules for basic processes are violated, and can never fall below 7 in the most general quark theory. However, the usual reduction in F due to nonscaling

behavior is consistent with the present data.

$\underline{P^{\pm}}$: The N_{eff}'s for p and $\bar{p}$ are very similar. The presence of N = 8 terms is clearly demanded by the CP data; N = 6 or 4 terms are also required by data in the ISR range. A single N = 8 term cannot fit both energy ranges. From the N_{eff} curves alone, it is not certain whether N = 4 terms are needed, but if one restricts $M_6^2 < 4\ GeV^2$, their presence is probably indicated. The situation becomes clearer by examining the F_{eff} curves which show a distinct difference between FNAL and ISR energy ranges.

The F_{eff} values in the ISR range for both p and $\bar{p}$ are distinctly higher than the values expected from minimal (nonscaling) processes with N = 6 or 8.

In the FNAL range at large p_T, F_{eff} for protons is consistent with a value 3 - 5. The value 5 is characteristic of the N = 6 process $q + (qq) \rightarrow B + M$, which is also seen in the $\pi^{\pm}$ and K^+ spectrum. The values 1 and 5 are consistent with proton CIM processes with N = 8. The N_{eff} curve clearly prefers the latter choice with $M_8^2 \sim 2.5 - 3\ GeV^2$. A single term with N = 8, $M_8^2 = 3\ GeV^2$, and a limiting F = 5 (the subprocess in $M + B \rightarrow M + B$) could account for the entire CP data range.[43] This extreme is probably in conflict with the strong N = 6 process seen in the pion data which simultaneously creates large p_T baryons and thus requires that a reasonable percentage of the protons arise from this mechanism. This is consistent with the N_{eff} curve if M_8^2 is small. The decreasing trend of F_{eff} should arise from the usual non-Feynman scaling effects.

One would be tempted to explain the BS-ISR data by the subprocess $q + q \rightarrow B + \bar{q}$ which has N = 4 and F = 7. However, it is difficult to achieve the sharp transition in the behavior of F_{eff} between ISR and FNAL with only this additional term. This effect, together with the rise of N_{eff} above 4 over the ISR range,

suggests that a term with $N = 4$ and large F ($\gg 7$, perhaps ~ 13), together with a term with $N = 6$ or 8 with a moderate F, are both important in the ISR energy range. The proton distributions are clearly the most complicated. Large p_T ISR data should help greatly to clarify the situation.

Although the kinematic range of the $\bar{p}$ extractions is limited, $N = 4$, 6, and 8 terms seem to be required. The minimal CIM F_{eff} value, for the $N = 6$ and 8 terms (which presumably dominate the FNAL data), is 11. The extracted F_{eff} values are consistent with this if non-Feynman scaling effects are present. Experiments capable of probing closer to $\epsilon = 0$ are clearly desirable. The higher F_{eff} values for the BS-ISR data again suggest the presence of important high F, $N = 4$ terms. The minimal $N = 4$ CIM value is $F = 11$ (from $q + \bar{q} \rightarrow B + \bar{q}$)and 15 (from other processes). In analogy to the proton case, the extracted F and N values in this region may be a result of a combination of high F, $N = 4$ terms and $F = 11$, $N = 6$ (and 8) terms. Much more experimental information will be needed to substantiate these hints from present data.

VII. CONCLUSIONS

As we have seen, the constituent interchange model, combined with quark counting rules, can give a simple accounting of many of the features of the inclusive data at large p_T. Among the successes of the CIM are:

(1) The plateaus for N_{eff} at the predicted values $N = 4$, 6 for meson production. The $N = 4$ terms with high F dominate at large p_T in the $\epsilon \sim 1$ ISR region, and the $N = 6$ terms with lower values of F dominate at the smaller ϵ FNAL energy range. There is also the probable presence of $N = 8$ terms for p or $\bar{p}$ production at FNAL.

(2) The relative ordering and values for $N_{excl} = F + N + 1$ for different produced particles.

(3) The general understanding of the shapes of F_{eff} and N_{eff} for particular particles.

(4) The quasielastic peak ($F_{eff} = 0$) in the ϵ distribution for (p-$\bar{p}$) and ($K^+ - K^-$) particle production differences. Further, for the peak values, $\epsilon_{ISR} > \epsilon_{FNAL}$, consistent with the greater number of spectators expected in the higher energy regime (and its higher F_{eff} values).

We reemphasize, however, that the comparisons with the present data are subject to the uncertainties of both statistical and systematic (especially nucleon target effects) errors, and further confirmations of the above effects are required.

Although the CIM makes a great number of specific predictions, it is difficult to ascertain the relative contributions of those basic subprocesses that have similar F and N values using only single particle inclusive cross section data. Correlation data between large p_T particles on both sides, including quantum number identification and angular distribution data, should be decisive

here. As we have seen, certain subprocesses demand that the balancing recoil system carries specific baryon or strangeness quantum numbers. In the case of the $qM \rightarrow qM$ subprocess, the system recoiling from the detected meson M has the same jet-like final state features as the quark parton system recoiling in deep inelastic lepton scattering. Alternatively, if the detected meson arises from fragmentation of the final state quark, one expects substantial same side correlation and a recoiling mesonic system. Note that for subprocesses such as $q + \bar{q} \rightarrow C + H$, the recoiling system H never has the same charge as C. See Section VI for further examples. We note that many features of the present correlation data, including the multiplicity patterns, are consistent with the structure of the hard scattering models, although the ϕ-noncollinear angular correlation may be uncomfortably broad. The predictions for same side correlations have not yet been fully worked out since they depend on the details of resonance formation. It has been pointed out by Sivers[44] that if the basic subprocess involves the production of a third particle, then the final state is not coplanar and the ϕ correlations will be broadened.

Another discriminant of the various contributing subprocesses is the angular distributions of the single particle inclusive data. In the forward (triple Regge) regions, the behavior for $x_L \sim 1$ reflects the spectators in the beam fragmentation region (see Ref. 9). The large angle cross sections depend on the angular structure of $\frac{d\sigma}{dt}(a + b \rightarrow c + d)$ as well as the distribution functions, as given in Eq. (II. 1). When a and b have strongly different distribution functions, such as q and $\bar{q}$ in p-p scattering, the resultant angular distribution is broad and most likely peaked away from 90°. Also, if the incident particles A and B are different, then one can distinguish between subprocesses that have a strong t or u dependence. A more detailed discussion of the subprocess

angular dependence in the CIM is given in Refs. 3, 4, and 9.

Among the most important tests of the CIM are the intercomparison of particle production using different beams and targets. Generally speaking, meson and photon beams are predicted to be more effective in producing particles at large x_T because of the fewer number of beam spectators; quasielastic peaks for differences of cross sections will be at smaller values of ϵ for mesons relative to baryons. The comparison of inclusive cross sections using π, K, p, $\bar{p}$ beams and proton or deuteron targets with the production of different particle types will further specify the most important subprocesses, and suitable double and triple differences can permit the isolation of the various components of the probability distribution. Since the Feynman-scaling contributions are particle-independent, such differences can be used to further isolate the valence quark content of the beam, target, and trigger. Note also that certain subprocesses are also eliminated by taking cross section differences, e.g., $q + \bar{q} \rightarrow p + \bar{p}$ cancels between the p and $\bar{p}$ production cross sections.

There are several important normalization checks that must be satisfied in the CIM. For example, the subprocess $q + (qq) \rightarrow M^* + B^*$ contributes equally to meson and baryon production, except for the differences in the sums over final state resonances. Another constraint arises from crossing symmetry. Any basic contribution to $A + B \rightarrow C + X$ will yield an analogous term in $\bar{C} + B \rightarrow \bar{A} + X$ which is expected to be of the same order of magnitude. The absolute normalization of CIM processes requires specific knowledge of the wave function and distribution functions involved. Information on these can be obtained from momentum sum rules, decay rates, asymptotic form factors, and structure functions in the threshold region. Thus far it has proved difficult to use the inclusive-exclusive connection as a normalization constraint mainly because

the inclusive data does not extend close enough to $\epsilon = 0$ and also the elastic data must be extrapolated to very large s. For instance, an attempte to normalize the contribution of the leading particle subprocess $q + p \rightarrow q + p$ to $pp \rightarrow pX$ cross section using the proton elastic data yields much too large an inclusive cross section (using the ratio of the form factor contribution to νW_2 in deep inelastic scattering). However, the process $qq + p \rightarrow qq + p$ alone yields a reasonable value.

Earlier it was pointed out that a model may provide an acceptable fit to the data but yet give a poor representation of F_{eff} and N_{eff}. The effective power analysis of the data is more sensitive to systematic features of the data. There are many additional applications of this data analysis technique beyond large p_T inclusive cross sections. These include:

a) $\ell p \rightarrow \ell X$, $e^+e^- \rightarrow HX$, $\mu p \rightarrow \nu X$, etc. If Bjorken scaling holds for $\ell p \rightarrow \ell X$, then the F_{eff} and N_{eff} analysis will yield $N_{eff} = 2$ (corresponding to the $\ell q \rightarrow \ell q$ subprocess) and $F_{eff} \sim 3$ which is the standard Drell-Yan prediction (two spectators). Interesting background terms arising from $\ell(qq) \rightarrow \ell(qq)$ with $N = 4$ and $F = 1$ can be important at small ϵ; their presence is usually hidden by using the ω' variable (see Section V), but they can be explicitly detected from the F_{eff} and N_{eff} plots. Note that radiative corrections in finite order do not affect the F values but change the overall energy dependence by logarithms.

b) $ep \rightarrow HX$ where H is produced at large p_T relative to the incident e. This unusual process is normally not studied, but it can clarify the roles played by various subprocesses. The two basic ones for meson production are $eq \rightarrow eq \rightarrow e(M+q)$ with $N = 2$, $F = 5$ and $\gamma q \rightarrow Mq$ with $N = 3$, $F = 4$. In the first case one has a correlated lepton recoil system, and in the second, a quark.

c) $\gamma p \to \gamma X$. The leading subprocess for large p_T is $\gamma q \to \gamma q$ with $N = 2$, $F = 3$ (see Ref. 1) and the leading one for $\epsilon \to 0$ is $\bar{q} B \to \gamma (qq)$ with $N = 5$ and $F = 0$. The latter term seems to dominate at the present (SLAC) energies (see Ref. 9 for further discussion of this reaction and inclusive photo-meson production).

d) $pp \to \mu X$. The Drell-Yan process $q\bar{q} \to$ "γ" $\to \mu^+\mu^-$ predicts $N = 2$, $F = 11$ but there are many other possible candidates. Since the present data[45] indicate a constant μ/π and ℓ/π ratio, hadronic production mechanisms are undoubtably important. Again, a detailed F_{eff} and N_{eff} analysis will help to determine the dominant production mechanisms.

In conclusion, we have seen that the CIM can explain both the form and detailed differences between the inclusive cross sections for various produced particles in a wide kinematic regime. Further tests of this approach will have to be of a much more detailed nature. Other theories of large p_T processes are not as fully developed as the CIM. We expect that a properly formulated Regge parametrization can be constructed that would account for the data if for no other reason than the fact that each contribution in this approach has two associated arbitrary functions $\beta(t)$ and $\alpha(t)$. Furthermore, the CIM has already been shown to develop Regge behavior and to predict the asymptotic behaviors of the residue and trajectory functions, and the proper threshold behavior in the triple Regge limit. It has far fewer parameters than a pure Regge theory.

The 90° region concentrated upon in this paper is most naturally associated with the pionization (central) region. The standard double Regge parametrization does not have the threshold factor ϵ^F which is prescribed in the CIM. The presence of such threshold factors in the model allows a unified description and smooth continuation throughout the entire Peyrou plot. The explicit powers

of x_1 and x_2, Eq. (V.8), do have direct Regge analogues which are present in the non-Feynman scaling terms.

The CIM in combination with the quark counting rules provides a beautifully simple hadronic model which incorporates the following desirable properties:

1) unified description of the entire Peyrou plot
2) correct crossing behavior for exclusive and inclusive amplitudes
3) smooth connection to Regge behavior in all appropriate limits
4) smooth inclusive-exclusive connection at any angle
5) the proper approach to Feynman scaling
6) the usual quark-parton model and Bjorken scaling
7) the quark degrees of freedom and thus the strong quantum number dependence and duality features of hadronic reactions.

The next crucial test of the CIM involves the consistency between the predicted values of F and N for various subprocesses and their associated correlations.

Acknowledgement

We wish to thank J. Bjorken, R. Raitio, G. Ringland, and D. Sivers for helpful conversations.

REFERENCES AND FOOTNOTES

1. J. D. Bjorken and E. A. Paschos, Phys. Rev. 185, 1975 (1969); R. P. Feynman, Phys. Rev. Letters 23, 1415 (1969); and R. P. Feynman, Photon-Hadron Interactions (W. A. Benjamin, Reading, Mass., 1972).
2. S. M. Berman, J. D. Bjorken, and J. Kogut, Phys. Rev. D 4, 3388 (1971); J. D. Bjorken, Phys. Rev. D 8, 4098 (1973).
3. J. F. Gunion, S. J. Brodsky, and R. Blankenbecler, Phys. Letters 39B, 649 (1972); Phys. Rev. D 8, 287 (1973); R. Blankenbecler, S. J. Brodsky, J. F. Gunion, and R. Savit, Phys. Rev. D 8, 4117 (1973); 10, 2153 (1974).
4. P. V. Landshoff and J. C. Polkinghorne, Phys. Letters 45B, 361 (1973); Phys. Rev. D 8, 927 (1973); 8, 4157 (1973).
5. S. J. Brodsky and G. R. Farrar, Phys. Rev. Letters 31, 1153 (1973) and SLAC-PUB-1473, Stanford Linear Accelerator Center (1974) (to be published in the Physical Review).
6. V. Matveev, R. Muradyan, and A. Tavkhelidze, Nuovo Cimento Letters 7, 719 (1973).
7. R. Blankenbecler, S. J. Brodsky, and J. F. Gunion, Phys. Rev. D 6, 2652 (1972); Phys. Letters 42B, 461 (1973).
8. P. V. Landshoff and J. C. Polkinghorne, Phys. Rev. D 8, 4157 (1973); Phys. Letters 45B, 361 (1973) and preprint DAMTP 73/22 (1973); Phys. Rev. D 10, 891 (1974).
9. R. Blankenbecler and S. J. Brodsky, Phys. Rev. D 10, 2973 (1974); J. F. Gunion, Phys. Rev. D 10, 242 (1974).
10. G. Preparata, CERN preprint TH 1859 (1974).

11. For recent reviews and other references see P. Landshoff, S. Ellis, V. Barger, and J. Gunion, Proceedings of the International Conference on High Energy Physics (1974); S. D. Ellis and R. Thun, IXe Recontre de Moriond (1974), CERN preprint TH. 1874 (1974); S. D. Ellis Vth International Symposium on Many Particle Hadrodynamics, Eisenach-Leipzig (1974); S. J. Brodsky, Proceedings of the Stony Brook Conference, the SLAC Summer Institute, SLAC-PUB-1497 (1974); R. Blankenbecler, IXe Recontre de Moriond (1974); R. Blankenbecler, preprint SLAC-PUB-1438 (1974), talk presented at the IXth Balaton Symposium on Particle Physics, Hungary (1974); Proceedings of the SLAC Summer Institute (1974); J. Bjorken, Aix Conference (1974); M. Jacob, CERN preprint TH. 1453 (1974); R. Blankenbecler, S. Brodsky, and D. Sivers, Phys. Reports (in preparation).

12. D. Amati, L. Caneschi, and M. Testa, Phys. Letters 48B, 186 (1973); M. Teper, Westfield College preprints (1974).

13. E. L. Berger and D. Branson, Phys. Letters 45B, 57 (1973); L. K. Chavda, and D. S. Narayan, Tata preprint (1974); A. Jabs, Trier-Kaiserlautern preprint (1975); S. Sakai, Tokyo preprint (1973).

14. Meng Ta-Chung, Phys. Rev. D 9, 3062 (1974); J. J. Dumont and L. Heiko, Louvain preprint (1974); A. Bouget et al., Orsay preprint (1974); M. Duong-Van and P. Carruthers, Phys. Rev. Letters 21, 133 (1973).

15. H. M. Fried and T. K. Gaisser, Phys. Rev. D 7, 741 (1973), D 4, 3330 (1971), D 6, 2560 (1972); A. P. Contogouris, J. P. Holden, and E. N. Argyres, Phys. Letters 51B, 251 (1974); I. G. Halliday, J. Haskins, and C. Sachrajda, Imperial College preprint (1974); H. M. Fried, Brown University preprint (1974).

16. F. W. Busser et al., CERN-Columbia-Rockefeller collaboration, Phys. Letters 46B, 471 (1973); see also J. A. Appel et al., Phys. Rev. Letters 33, 719 (1974).

17. B. Alper et al., British-Scandinavian collaboration, Phys. Letters 47B, 75 (1973); see also M. Banner et al., Saclay-Strasbourg collaboration, Phys. Letters 44B, 537 (1973).

18. J. W. Cronin et al., Chicago-Princeton collaboration, Phys. Rev. Letters 31, 1426 (1973); Chicago-EFI preprints 74-1181 and 74-1182 (1974); J. W. Cronin, Proceedings of the SLAC Summer Institute (1974); see also, D. C. Carey et al., Phys. Rev. Letters 32, 24 (1974).

19. Also see, S. D. Ellis and M. B. Kislinger, Phys. Rev. D 9, 2027 (1974); D. Cline, F. Halzen, and H. Waldrop, Nucl. Phys. B55, 157 (1973); D. Horn and M. Moshe, Nucl. Phys. B48, 557 (1972), B57, 139 (1973).

20. M. Bander, R. M. Barnett, and D. Silverman, Phys. Letters 48B, 243 (1974); S. D. Ellis, Phys. Letters 49B, 189 (1974).

21. The use of the parameter N_{eff} is discussed by J. Cronin in the proceedings of the SLAC Summer Institute (1974).

22. For an analysis of large t, large u exclusive data, see R. Blankenbecler, D. Coon, J. Gunion, and T. Van Than, SLAC-PUB-1483, Stanford Linear Accelerator Center (1974).

23. This is the correspondence principle of J. Bjorken and J. Kogut, Phys. Rev. D 8, 1371 (1973). Equation (VI. 14) is discussed in Refs. 5, 9, and D. M. Scott, preprint DAMTP 73/37 (1973).

24. Nuclear effects are discussed by G. Farrar, Caltech preprint (1975); J. Pumplin and E. Yen, Michigan State preprint (1975); and S. Frederiksson, Stockholm preprint (1975). No compelling explanation of the observed A dependence has been given.

25. Reference 16 quotes the value $\langle N_{eff} \rangle_{\pi^0} = 4.12 \pm 0.03$ (± 0.35 including systematic errors).

26. M. Ta-Cheng, Ref. 9.

27. L. Heiko et al., Ref. 9.

28. D. Amati et al., Ref. 12.

29. See, e.g., R. Barnett and D. Silverman, Phys. Rev. D 10, 1510 (1974).

30. Note that the statistical approach to particle ratios discussed by J. Bjorken and G. Farrar, Phys. Rev. D 9, 1449 (1974) should be valid only for large p_T and very small x_T. Since not all particle ratios are x_T independent at fixed p_T over the current experimental range it seems that the necessary kinematic regime has not been reached.

31. R. F. Cahalan, K. A. Geer, J. Kogut, and L. Susskind, Cornell preprint CLNS-289 (1974).
See also J. Gunion, Proceedings of the XVII International Conference on High Energy Physics, June 1974.

32. The result for $G_{\bar{q}/p}$ was derived and used for the parametrization of the nucleon structure functions by G. Farrar, Nucl. Phys. B77, 429 (1974) and J. F. Gunion, Ref. 9.

33. Equation (IV.8) correctly connects $A+B \rightarrow C+X$ to $\bar{A}+B \rightarrow \bar{C}+X$.
This is discussed further in R. Blankenbecler, S. Brodsky, and D. Sivers (to be submitted to Physics Reports).

34. In the language of J. Gunion, Ref. 9, particle bremsstrahlung of an electron (either by pair creation with associated photon emission) requires only one uncompensated large energy denominator in the limit $x \rightarrow 1$ for each additional spectator. In contrast, for hadrons every spectator is assumed to have also appeared in the initial hadronic state. This implies two large uncompensated

energy denominators per spectator. The results for quantum electrodynamics agree with the endpoint behavior of the usual equivalent photon and lepton expressions. (M. C. Chen and P. Zerwas, private communication.)

35. This crossing property is verified in pseudoscalar field theory model by M. Roth, University of Illinois preprint TH-74-10 (1974).

36. For example, the tabulated F value for $pp \to \bar{p}X$, arising from the basic process $q_1 + M_1 \to q_2 + M_2$, is computed as follows: there are two spectators associated with the emission of q_1 from an incident nucleon and three associated with the emission of q_1 from an incident nucleon and three associated with M_1. The fragmentation of M_2 into a $\bar{p}$ requires at least three final spectators. Thus $N_{passive} = 8$ and hence $F = 15$.

37. Equation (V. 1) also provides a convenient covariant form for the calculation of the two photon process $ee \to eeA\bar{A}$. In this case the F's are computed from the equivalent photon approximation.

38. A simple realization of coherent sum which gives Regge behavior is

$$G^{(\lambda)}_{a/A} = \sum_{\delta=91\ldots} \frac{\left[\lambda(1-x)^3 \log \frac{1}{x}\right]^\delta}{\delta!} (1-x)^{2n(\bar{a}A)-1} x^{2n_a-1} ,$$

which matches with the endpoint behavior of Eq. (V.6) if $h=2n_a-1-\lambda=-\alpha$. This form shows that the contribution from an extra spectator quark pair vanishes faster by a factor $(1-x)^4$ at $x \to 1$. This form for Regge behavior is typical to what is obtained from summing ladder graphs in field theory, as shown, for example, in the pseudoscalar model by S. Drell, D. Levy, and T. M. Yan, Phys. Rev. D 1, 1035 (1970). Examples of valence structure functions which vanish at x=0 are also discussed here and in Refs. 1 and 39.

39. J. F. Gunion, Ref. 9.

40. In order to illustrate the effects of the exact integration using detailed distribution functions, we have computed Eq. (V. 1) directly, employing the nucleon's quark distribution extracted from the data in Ref. 39, convoluted with a representative $(1-x)^5$ distribution. The result is that F_{eff} is close to the minimal value F=9 through most of the range of ϵ, but is 1 or 2 units less at $\epsilon \sim 1$. To the extent that the shape of νW_2 and the behavior of the latter calculational example are representative, it is unlikely that a given F_{eff} will ever rise substantially above its $\epsilon \rightarrow 0$ limit.

41. F. W. Busser et al., CERN preprint (1974).

42. F. W. Busser et al., Phys. Letters D55, 232 (1975).

43. Such processes are discussed by M. Teper, Ref. 12.

44. D. Sivers (private communication).

45. J. P. Boymond et al., Phys. Rev. Letters 33, 112 (1974).
J. W. Appel, FNAL preprint 74/71 (1974); F. W. Busser et al., Phys. Letters 48B, 371 (1974).

LIST OF FIGURES

1. The structure of $A+B \rightarrow C+X$ at large transverse momentum in the hard scattering models. The active particles a, b, c, or d can be quarks, hadrons, leptons, or photons depending on the model and process. The contributing large angle subprocess $a+b \rightarrow c+d$ is irreducible: no further bremsstrahlung from a, b, or c is allowed.
2. The parameters F_{eff} and N_{eff} (see Eqs. (II. 2) and (II. 3)) obtained from the $pp \rightarrow \pi^0 X$ ISR data of CCR collaboration, Ref. 16. Three energy pairs are used as indicated, with $p_T > 2.5$ GeV. The statistical errors are of the same size as the discrepancies from the different energy pairs. The prediction of the CIM is $N_{eff} = 4$ for this kinematic range.
3. The parameters F_{eff} and N_{eff} for charged hadron production at the CERN-ISR BS Collaboration, Ref. 17, pp collisions and the FNAL CP Collaboration, Ref. 18, $p_L = 200$, 300, 400 GeV proton-Tungsten collisions obtained using Eqs. (II. 1) and (II. 2). The energy pairs for the ISR (connected by wavy lines) are ($\sqrt{s} = 30.6 - 44.8$ GeV), and ($\sqrt{s} = 44.8 - 52.7$ GeV). The energy pairs for the FNAL (connected by straight lines) are ($\sqrt{s} = 19.4 - 23.8$ GeV) and ($\sqrt{s} = 23.8 - 27.4$ GeV). A p_T dependent nuclear correction is assumed for the FNAL data (see Section II). Only $p_T > 2$ GeV/c data are used.
4. Effects of finite mass corrections in $\left(p_T^2 + M^2\right)^{-N}$ upon N_{eff} (see Eq. (IV. 16)). The results are shown for $\sqrt{s} = 50$ and 25 GeV and $M^2 = 1$, 2, or 3 GeV^2.
5. The extraction of F_{eff} for the difference of the p and $\bar{p}$ production cross sections and the difference of the K^+ and K^- production cross sections at the ISR[17] (BS Collaboration) and FNAL[18] (CP Collaboration). The points are labelled as in Fig. 3. A zero value for F_{eff} indicates a quasi-elastic peak in the ϵ distribution (see Section V).

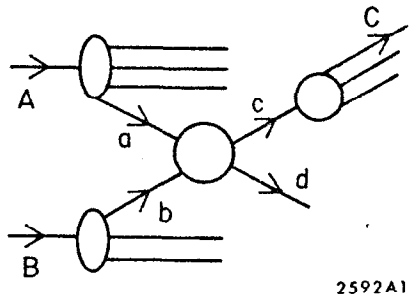
A
B
a
b
c
d
C
2592A1

Fig. 1

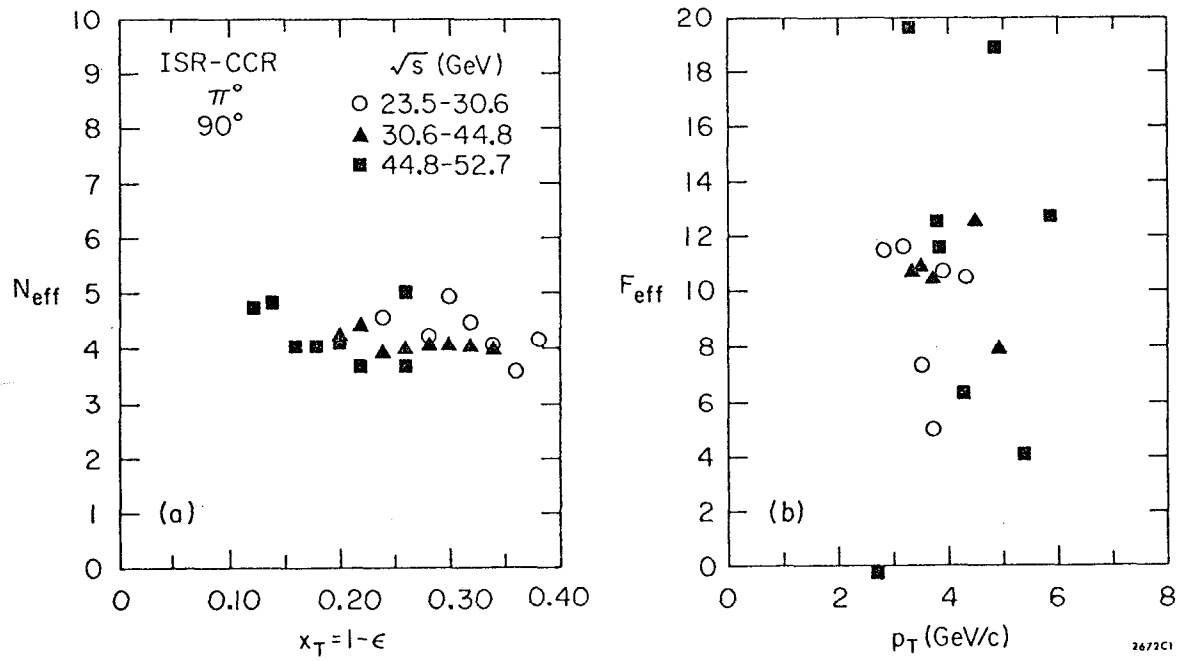
ISR-CCR
π°
90°
√s (GeV)
23.5-30.6
30.6-44.8
44.8-52.7
N_eff
(a)
x_T = 1 - ε
F_eff
(b)
p_T (GeV/c)
2672C1

Fig. 2

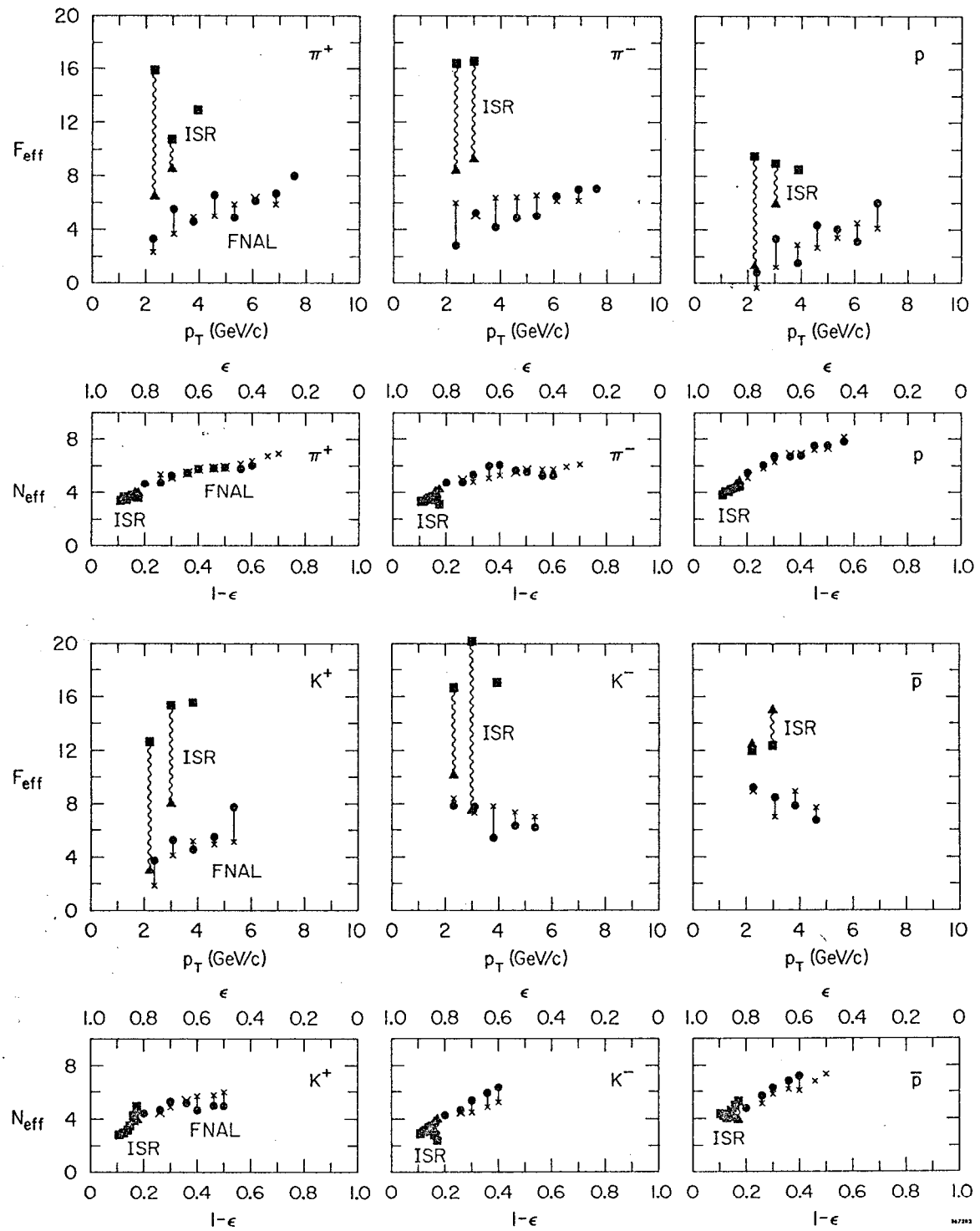

Fig. 3

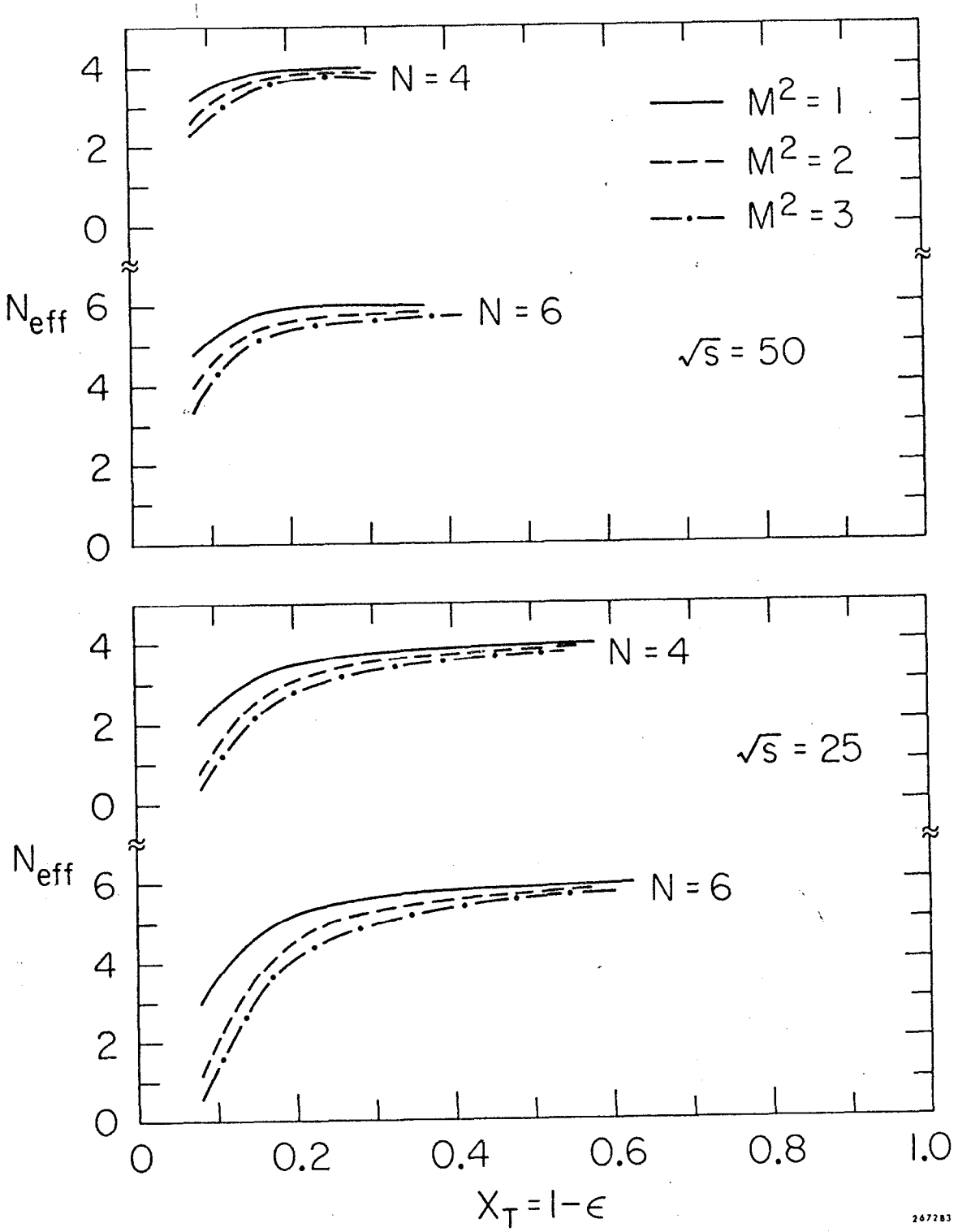
N = 4
$M^2 = 1$
$M^2 = 2$
$M^2 = 3$
N = 6
$\sqrt{s} = 50$
N_{eff}
N = 4
$\sqrt{s} = 25$
N = 6
N_{eff}
0
0.2
0.4
0.6
0.8
1.0
$X_T = 1 - \epsilon$
267283

Fig. 4

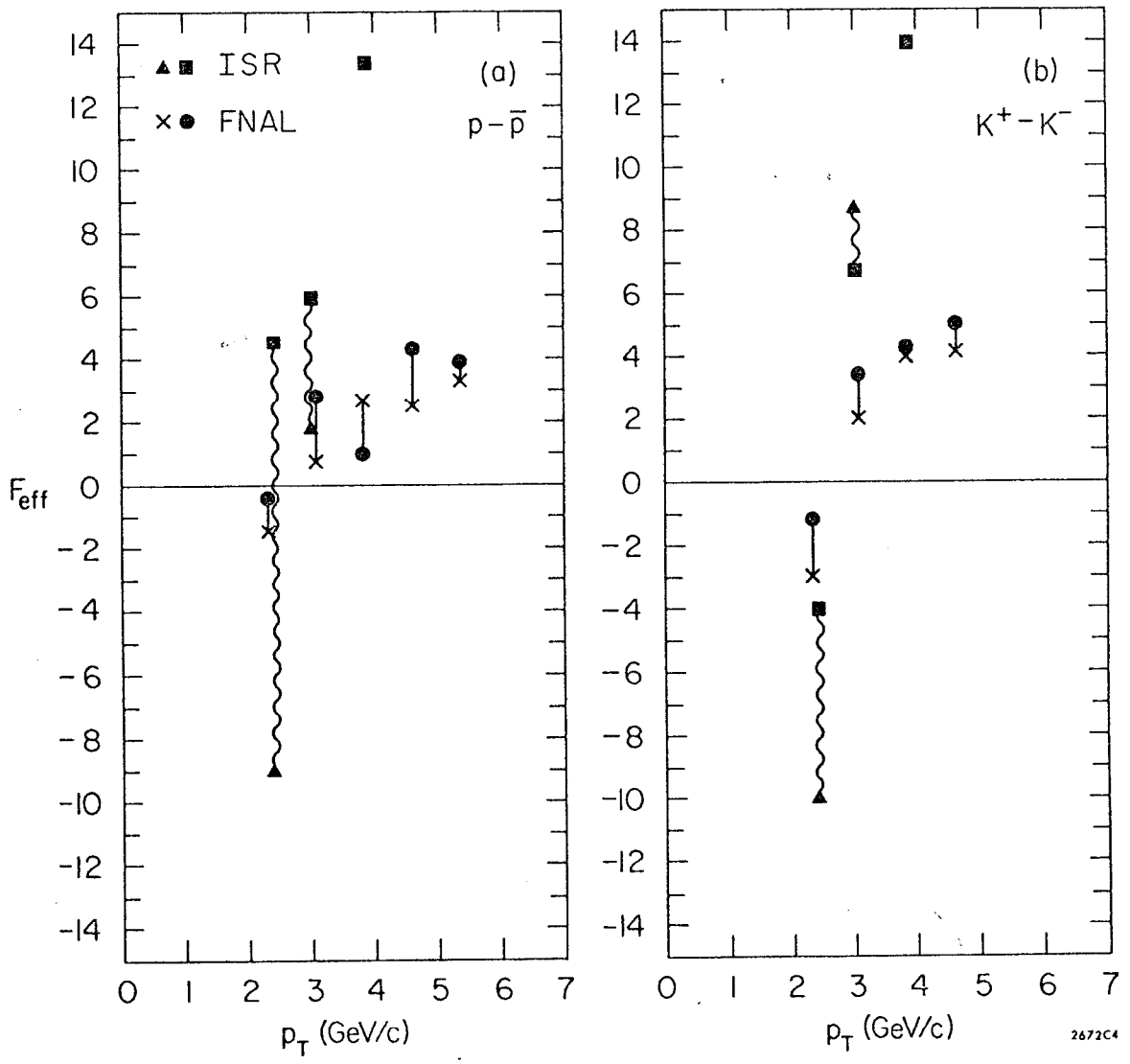

Fig. 5